Semiconductor microlasers with intracavity microfluidics for biomedical applications

P. L. Gourley and A. E. McDonald

Sandia National Laboratories, Albuquerque, NM 87185

ABSTRACT

Microfabricated electro-optical-mechanical systems are expected to play an important role in future biomedical, biochemical and environmental technologies. Semiconductor photonic materials and devices are attractive components of such systems because of their ability to generate, transmit, modulate, and detect light. In this paper we report investigations of light-emitting semiconductor/glass microcavities filled with simple fluids. We examine surface tension for transporting liquids into the intracavity space and study the influence of the liquid on the spectral emission of the microcavity.

keywords: microfabrication, microfluidics, semiconductors, glass, microcavities, lasers, spectroscopy, biomedical, cells, surface tension, capillarity, micro-optical-electrical-mechanical systems

1. INTRODUCTION

Recent progress in materials microfabrication has made it possible to consider developing chemical, biological, and physical analytical systems that can be integrated on a single substrate.[1-4] A common theme among these systems is the use of microfabricated substrates and use of micro-electro-optical-mechanical devices to manipulate specimens and derive useful information from them. Various names have been given to these systems including total microanalytical systems, chem-lab on a chip, and MEMS (micro-electro-mechanical systems) for biomedical applications. Almost all of these systems include a means for introducing fluid specimens into a separation channel or chemical reaction area, and incorporate a method for detecting various chemical or biological species. Two basic approaches to system design are microflow of specimens through a channel with a fixed point detector[2,3] or reaction of a fluid with substrate and parallel readout with scanned electronic or optical readout.[4]

A critical issue in the development of such systems is the choice of materials. Materials that can perform many functions and are easily microfabricated will become the material of choice for future applications. Currently, a wide variety of materials and materials combinations are under consideration. These include glasses, polymers, elastomers, semiconductors, and metals.[5] Glasses are attractive because they have long been used in capillary electrophoresis and are widely available. Semiconductors are attractive because of the extensive development of microfabrication technology. New uses of silicone elastomers are appearing. When considering electronic, optical, chemical and mechanical properties, each of these materials has certain advantages and limitations. Integrating materials requires methods for bonding, mechanical and chemical compatibility, electrical conduction and optical transparency properties.

Semiconductor photonic materials and devices are attractive components of such systems because of their ability to generate, transmit, modulate, and detect light.[6] In this paper we report investigations of semiconductor/glass microcavities for use in analyzing fluids. In particular, we investigate surface tension for transporting fluids into the cavity and study the influence of the fluid on the spectral emission of the cavity.

2. SEMICONDUCTOR PHOTONIC DEVICES

Semiconductor microtechnology is rapidly expanding its role in communications, information, and biomedical uses. The technology is mostly centered around the material silicon which is well developed for electrical devices for switching, memory, and light reception. Beyond these uses, silicon serves as an excellent material for microfabrication of microfluidic devices, micro-test tube arrays for pharmaceutical development, and implantable biomedical devices.[1] All of these advances have been enabled by concurrent developments in materials science, microlithography, and material processing. Compound semiconductors, derived from columns III and V of the periodic table are becoming important technologically for their ability to generate, transmit, modulate, and detect light. These compounds like GaAs, AlAs, InP, etc. have undergone extensive research and development in the last decade and are beginning to show remarkable potential for new biomedical applications such as photodynamic therapy,[7] optical tomography,[8] cell micromanipulation,[9,10] and laser cytometry.[11,12]

DISCLAIMER

2.1 A biological microcavity laser

GaAs surface-emitting lasers[13-16] have recently been used in a new method for analyzing biological cells. The method employs a semiconductor laser with a single human cell acting as an internal component of the laser. The cell actually aids the light-generating process, so the emitted laser beam is impressed with information about the cell. The new "biological microcavity laser" provides the basis for new biomedical analyses of cell structure. This includes both living and fixed cells from humans, animals, and plants. And, the technique doesn't require the customary chemical staining procedure to render its structure visible. Further, the cells can be connected in tissues, so long as the tissue is thinned to monolayer dimensions to fit within the laser cavity. Thus, the laser has potential uses for a novel kind of microelectronic cytometry and histopathology.

2.2 Applications

This intracavity laser technique provides coherent light spectra and images of cells and intracellular structures and has several critical advantages over conventional cell analysis methods. In preliminary experiments, the laser has shown potential to probe the human immune system (caliper cell and nucleus dimensions of lymphocytes),[14] characterize genetic disorders (quantify sickled and normal red blood cell shapes),[15] and distinguish cancerous and normal cells from tumors[3] It may be useful for pharmaceutical development in high-speed drug testing of living cells, or finding rare cells in large populations. A practical cytometer could operate in two basic configurations: either as a flow device or as static fluid device scanned by a probe laser.[16] Individual cells could be examined in detail or large populations of cells could be rapidly studied by flow combined with laser-scanning. Conventional flow cytometers tend to large, expensive instruments requiring highly trained operators. A microelectronic cytometer may be relatively inexpensive to manufacture, easy to operate, and permit accurate assessment of cell structure. Such technology may also aid the histopathologic examination of tumors. Conventional methods of sectioning, staining, and microscopic examination of abnormal cells rely on qualitative human vision and interpretation of color images. These methods are operator dependent and subject to frequent misidentification. Improvements brought by a microelectronic laser technique have the potential advantages of high speed automation, accuracy, and low cost.

2.3 Physics of the microcavity laser

The microcavity laser technique confines intense light inside the cell. Living or fixed cells are placed on a microfabricated AlGaAs/GaAs surface-emitting semiconductor wafer and covered with a glass dielectric mirror to form a laser resonator (see Fig. 1a). In this arrangement, the cells serve as optical waveguides (or lens elements) to confine (or focus) light generated in the resonator by the semiconductor. The waveguiding effect is due to slight differences in the dielectric constants between various cell components and the surrounding fluids.[17-18] These variations arise from different protein or DNA/protein concentrations in the cytoplasm, nucleus or organelles. The laser operates at resonant frequencies established by the dielectric properties of the cells. By using a high resolution spectrometer, these lasing frequencies can be resolved into narrow spectral peaks. The spacing and intensity distribution between peaks provides a unique spectral signature for each different cell as shown in the margins of Fig. 1c for normal red and white blood cells, platelets, and cancer cells.[13]

Each cell has a unique spectral signature that cannot be confused with other cells. This situation is analogous to identification of musical instruments based on their unique sounds comprising mixture of acoustical overtones. These results were used to develop the 3-D cluster plot method[13] for identifying cells illustrated in Fig. 1c. The cells can be distinguished on the basis of spectral features without need of images. This result has significant implications. Cell identification can be quantified by computer algorithms that process 1-dimensional spectra rather than complex, data-intensive 2-dimensional images. Consequently, higher cell identification rates can be achieved.

2.4 Advantages and technical hurdles

Considerable advantages over existing technologies are possible with this microcavity laser sensor. It can be operated at very high frequencies since the light is generated by a stimulated emission process. Photons generated by the semiconductor sample the cell hundreds of times as they bounce between opposing mirrors. This multiple sampling serves to amplify subtle refractive, absorptive or diffractive effects in the cell. T he durations of the light pulses are limited only by the speed of light traversing the cavity. With state-of-the-art mirror scanning and light detection methods, large populations of cells can be sampled in a short period of time (see Fig. 1b).[16]

Further, the stimulated emission occurs in a narrow beam that can be directed toward a small area, high speed detector. Thus, the light collection process is simple and efficient. And, the light signal is very intense providing high signal-to-noise ratio and enhanced signal sensitivity. The top dichroic mirror is reflective in the near infrared 850 nm, but transparent in the UV and visible. Thus, the cells can be probed with other light wavelengths, say from fluorescent tags,[19] while the cell is supporting lasing.

Major technical hurdles that must be cleared to make a practical microcavity laser cytometer include the following: Methods for reliably transporting fluids on and off the semiconductor wafer must be developed. This includes buffer solutions, stimulants, and the fluid media carrying the cells. All of this must occur without clogging the microplumbing leading to the analysis chamber. Biocompatibility of the glass and semiconductors is another issue that must be addressed. The semiconductor surfaces must be passivated with inert materials that won't alter the cells. And, the materials must be robust to withstand enzymes that may attack the surfaces. Another hurdle is the development of sealing methods for dissimilar materials to prevent cross-contamination from different microflow channels. The integrity of these seals must be retained over the lifetime of the device, such that the physical dimensions of the laser microcavity remain constant.

In the following sections, preliminary investigations of fluid dynamics in a microcavity are presented. The effects of surface tension and evaporation on fluid filling and purging are characterized. The influence of fluid motion on the cavity spontaneous emission spectrum is examined by studying the static and dynamic interaction of the fluid with cavity modes. In the discussions, materials issues for optical microfluidic devices are identified.

3. MICROFLUIDIC SURFACE-TENSION IN MICROCAVITIES

The microcavity laser is formed by bringing semiconductor and glass surfaces together. The intracavity space between these surfaces is a critical parameter for the operation of the laser. It is typically a few microns. Larger spacings create more diffraction loss, lower cavity Q, and higher pumping thresholds for lasing. A cavity spacing of a few microns also gives the narrowest possible spontaneous emission linewidth. Such small spacings cause difficulty in transporting fluids into the intracavity space. A channel cut less than 10 microns into the glass surface becomes more difficult to wet after it has been fabricated. The fabrication sealing process, fusion or gluing, usually modifies the channel surfaces leaving them in a non-wettable condition. If the channel is sufficiently large, surfractant solutions can be forced by pressure or sonication into the opening to make a wettable surface. If the channel is very shallow, it is difficult to force the surfractant into it.

An alternative approach is to create a wicking bridge inside the microcavity as illustrated in fig. 2. In this scheme, two large channels are micromachined into the glass surface which is usually a multilayer dielectric mirror on a glass substrate. The channels are large, 500 microns and are separated by a few hundred microns to form a bridge structure. The semiconductor wafer is placed over the bridge and bonded, covering the width of both channels but leaving the ends of both channels exposed. The portion of the bridge in contact with the wafer forms an intracavity space that can be fed by microcapillary action. This action occurs when a microdrop of fluid is placed onto the exposed bridge next to the wafer. The microdrop can be applied with a fused silica microcapillary tube abutting the wafer edge on the bridge as shown in Fig. 2b and 2c. The fluid can be delivered through a syringe or micropump off the chip (not shown in Fig. 2).

3.1 Kinetics of capillary feeding of the microcavity

When the droplet is applied to the bridge, it is wicked into the cavity at a rate determined by the cavity thickness L, viscosity of the fluid η, surface tension τ, and contact angle α associated with the surface wetting. In the simplest analysis, the equation of motion is

$$xw\tau\cos\alpha / L = -yw\eta\, dv/dx \qquad (1)$$

where y is the fluid penetration into the cavity and v(x) is the velocity profile normal to the cavity surfaces and w is the width of the bridge. After integrating this equation, the effective velocity of the fluid front in the cavity can be approximated as

$$v(y) \approx (L/12y)\,(\tau/\eta)\cos\alpha \qquad (2)$$

The prefactor is a penetration aspect ratio of the cavity and has an average value of 10^{-4} for typical experimental parameters of L=3 μm and $\langle y\rangle$=2.5 mm. The natural velocity $\tau/\eta = 7\times10^{3}$ cm/s and $\langle\cos\alpha\rangle$ is 0.48. Eqn 2 predicts a velocity of 0.34 cm/s that is

independent of the bridge width w.

3.2 Experimental measurements of capillary feed velocity

Microbridge structures shown in Fig. 2 were fabricated with widths of 200, 700, and 1000 microns and lengths of 5 mm. The microbridges were filled with water/dye solutions using capillary action and the average velocity of the fluid meniscus was measured. Two different cavity lengths, 3 and 100 microns were investigated. The observed velocities were 0.2 and 3 cm/s, respectively, demonstrating that the velocity increases with L as in Eqn 2. Further, the velocity was independent of bridge width. Widths smaller than 200 microns may influence the velocity, but were not investigated here.

To further test the experimental dependence of v on L, the velocity at a fixed value of y was measured for a water solution injected into a microcavity formed with two wide (2.5 cm) glass surface separated with a spacer of dimension 3 to 300 μm. The velocity, normalized to y=3 mm, is shown as function of L in Fig. 3. As predicted by Eqn 2, the velocity increases linearly with the spacer thickness L. A least squares fit gives v = 0.077 L (μm) cm/s. The absolute value of the velocity is slightly less than that predicted by Eqn 2.

The semiconductor/glass velocities are slightly less than that for the glass plates, due to a higher wetting angle for semiconductor compared to glass. For comparison, a channel, 17 microns deep and 700 microns wide, microfabricated between glass plates was also tested. The measured velocity (open circle) was 0.23 cm/s and falls well below the other data. The lower value is mainly due to surface roughness from etching (~few hundred nm observed by Fizeau interferometry) and increased contact angle from bonding the glass surfaces. And, it should decrease some 33 % due to additional shearing forces from the channel walls.

3.4 Fluid evaporation from the microcavity

The bridge lengths are about 0.5 cm so the filling time for the microcavity is a few seconds. Once the microcavity is filled, the fluid can be studied using by intracavity laser techniques until it evaporates from the sides of the bridge. Or, the fluid can be quickly purged from the cavity in a few seconds by flowing pressurized inert gas through the open channels surrounding the microbridge. With pressured gas, a cooling effect occurs and the microcavity temperature changes. The evaporation time of the fluid out of the microbridge is dependent on several factors. These include the exposed surface area of the fluid near the bridge boundaries, the flow rate of gas through the surrounding channels, and the temperature. Experimentally it was observed that the fluid evaporated from the intracavity space with an air/fluid meniscus that moved across the bridge, from the narrow gap to larger gap region. This variation in gap thickness was due to slight wedging of the cavity. The velocity of the meniscus decreased from 0.5 cm/s for the 200 micron bridge to 0.05 cm/s for the 1000 micron bridge. Thus the evaporation time to clear the fluid is inversely related to the width of the bridge and the volume of fluid on it. The effective surface evaporation rate can be determined from these measurements. The mass lost per unit area per second is

$$S=\rho wLv/2L(w+\ell) \approx \rho wv/2\ell \qquad (3)$$

where ρ is the fluid density and ℓ is the bridge length. Evaluating this expression for typical experimental parameters we find $S= (1 m\ell/cm^3)(0.1 cm)(0.05 cm/s)/2(0.5 cm) = 5 u\ell/cm^2s$.

4. INTRACAVITY SPECTROSCOPY OF MICROFLUIDS

As described in section 2 the emission spectrum of the microcavity is useful for characterizing cells and particles in the cavity. The transverse optical modes defined by these transparent objects are evident in the emission spectrum. Such modes are experimentally observed for objects as small as 1 micron. Smaller particles modify the intensity and linewidth of the longitudinal modes of the Fabry-Perot cavity, but do not allow distinct transverse modes. Molecular and ionic solutions will also alter the emission spectrum, due to light absorption, scattering and refractive index changes. As the fluid index increases, both the optical pathlength and the wavelength of the longitudinal modes increase. By monitoring the modes through the emission spectrum, changes in the refractive index of the fluid in the microcavity can be determined. Further, the emission spectra can monitor mechanical changes of the cavity when fluids are introduced or removed. Thus, the microcavity can serve to detect changes in fluid composition and dynamics of the fluid/cavity interactions.

4.1 Experimental spectra and mode dynamics

Typical emission spectra from the microcavity with air (n=1.00) and an infrared laser dye in ethylene glycol (n=1.425) are displayed in Fig. 4. These spectra reveal two dominant longitudinal modes in the region between 790 and 850 nm. The peaks have very high signal-to-noise ratios, the order of 100-to-1, making their detection unambiguous. Shifts in peak wavelength or peak shape are easy to monitor as conditions of the cavity are changed. The peak positions in the bottom dye spectrum are shifted with respect to the air spectrum because the resonance condition changes when the cavity is filled with fluid. The peaks occur at different wavelengths, and they have a much smaller spacing.

To illustrate how these peaks can detect cavity changes, we show the effects of natural evaporation of water from a water-filled cavity, from wet to dry condition, in Fig. 5a. In the top figure, the evaporating water in the cavity is followed for 12 minutes. During this time, the air/water meniscus moved through the emitting region of the cavity. At short times the wet cavity displays a mode near 855 nm. As the meniscus passed through the emitting region, an abrupt and large mode jump was observed. A new mode near 848 nm appeared in the dry cavity near a time of 6 min. This mode remained constant in wavelength for the duration of the measurements.

The effects of cavity warming after purging a water-filled cavity with pressurized gas are illustrated in Fig. 5b. Initially, the cooled cavity exhibits a mode near 836 nm. Within a few minutes the cavity is warmed to room temperature, and the mode shifts to near 848 nm. At longer times the mode remains stable. The magnitude of this shift indicates that the cavity had been cooled significantly ~50C. The shifting of the mode with temperature is due primarily to differential thermal expansion the cavity materials and attendant changes in cavity length. Thus, the data of Fig. 5 show how changes in the cavity due to the presence of different fluids and temperature can be monitored by the emission spectrum.

4.2 Theoretical longitudinal mode wavelength and mode spacing

It is of interest to determine how sensitively the mode wavelengths depend on the refractive index of the fluid. The longitudinal mode wavelengths are given by

$$\lambda_m = \xi/(m-\phi/2\pi), \tag{4}$$

and the mode wavelength separations are given by

$$\Delta\lambda_m/\lambda_m = -(\lambda_m/\xi)/[1+\lambda_m\xi'/\xi + \lambda_m^2\phi'/2\pi\xi] \tag{5}$$

where $\xi=2\Sigma\ell_i n_i$ is the roundtrip optical pathlength in the cavity comprising a sum of lengths ℓ_i of index n_i (here including a fluid region $\ell_1 n_1$ is and a semiconductor gain region $\ell_2 n_2$), ϕ is the sum of the mirror phases, and the primes denote derivatives with respect to wavelength.

The mode lineshape can be approximated by a Lorentzian function of linewidth $\Delta\lambda=-\lambda^2\gamma/2\pi c$, where

$$\gamma = \gamma_m + \gamma_s + \gamma_d + \gamma_f \tag{6}$$

and the terms on the right denote mirror leakage and scattering, semiconductor absorption, cavity diffraction, and fluid absorption and scattering, respectively. The linewidth is also affected by the instrumental resolution. Typical linewidths in Fig. 4 are a few nm.

Typically, the fluid region has an effective pathlength of (3μm)(1.33)= 4 μm and the semiconductor region pathlength is (0.4μm)(3.5)= 1.4μm. Thus the fluid region is about 3 times the optical thickness of the active region. Eqn (4) indicates that the mode wavelength changes linearly to the refractive index change as $d\lambda_m/\lambda_m dn_1 = \ell_1/(\ell_1 n_1 + \ell_2 n_2)$. The smallest detectable change in wavelength is about 0.01 nm corresponding to an index change of about 10^{-5}. In Fig. 4, the wavelength shift of a given mode from dry to wet conditions is about 250 nm, larger than the spectral range displayed. Thus, the modes observed in the lower spectrum have much higher index values m.

Eqn (5) shows that the mode spacing is inversely related to the path length and will decrease as the fluid index increases. This effect is shown in Fig. 4 where the mode spacings for a dry and wet cavity as 50 and 30 nm, respectively. The magnitude of the mode spacing is dependent on wavelength and is governed by the wavelength dispersion of the pathlength and mirror phase. The dispersion

of the fluid index is negligible compared to that of the semiconductor and the mirror phase. The former quantity has been measured and the latter is readily calculated. The semiconductor dispersion is large and negative (positive) in the region near and below (above) the bandgap where the microcavity emits. The mirror phase is approximately a linearly decreasing function of wavelength near the reflectance zone center. It has a negative dispersion above and below the bandgap wavelength. According to these dispersions, we expect the mode spacing to be larger below the bandgap and smaller above it.

4.3 Influence of the cavity spacing on mode wavelengths

Experimentally, the mode wavelengths were measured by recording emission spectra from the microcavity. The measured wavelengths are primarily sensitive to the physical spacing of the cavity ℓ_1 and the fluid index n_1. If the temperature changes, then changes in the semiconductor index n_2 and the mirror phase will alter the wavelength. It is possible that other physical effects can alter the cavity spacing, and we consider some here.

4.3.1 Effects on surface tension on cavity spacing

When the cavity is filled with fluid, we expect surface tension to draw the semiconductor and glass together. Usually the semiconductor wafer (about 500 μm thick) is much thinner than the glass substrate (3 to 6 mm thick) and can flex if both surfaces are not perfectly flat. The pressure exerted on the surfaces is $p=\tau S/A$ where S is the circumference of the fluid meniscus, and A is the wet contact area. For a typical microbridge, S=0.8 cm, A=0.03 cm^2 and τ=72 dyne/cm so p=2000 dyne/cm^2 about 500 times smaller than atmospheric pressure. The deflection of the semiconductor in the bridge area is $\delta=pA\ell^3/192EI$ where ℓ= 0.5 cm is the length of the semiconductor piece, A is the wet contact area of the microbridge, $E=3\times10^{12}$ dyne/cm is Young's modulus, and $I=bd^3/12=(0.3\text{cm})(0.05\text{cm})^3/12 = 3\times10^{-7}$ cm^4 is a moment of inertia, where b and d are the width and thickness of the wafer, respectively. The deflection due to surface tension is δ=4Å. Thus $\delta\lambda_m/\lambda_m = 0.75(4/3\times10^4) = 10^{-4}$, or $\delta\lambda_m$=0.8Å. This change can be detected in the spectra, but is a very small effect.

Another cause for cavity length changes is variations in the mechanical forces that hold the semiconductor to the glass. The cavity can be simply pressed together with rigid or compliant materials or sealed with a glue or wax. In the former case, modification of the holding forces due to relaxation in the clamping materials can occur. In the later case the holding seal can be weaken, or flex, or crack, and relax the bond. We expect that the relaxation would lead to an increase in the cavity space and an increase in mode wavelength.

4.3.2 Experimental mode wavelengths vs cavity spacing

Fig. 6a shows the experimental mode wavelengths as a function of cavity air spacing from 0 to 6 μm. The cavity was intentionally wedged to create the spacing variation. The spacing was determined by observing cavity interference fringes with visible light and is accurate to within 1/10th wave or about 80 nm. In Fig. 6a, these data resemble a series of S-shaped curves. Each curve corresponds to a fixed mode index m. The curves slant toward the right, showing that the mode wavelength increases with cavity spacing as predicted by Eqn 4. The central portion of each curve is linear. Away from the center, the mode wavelength changes more rapidly with cavity spacing. This increase in slope occurs near the edges of the high reflectance zone where the mirror phase changes more slowly with wavelength. Here the optical intensity in the cavity extends further into the multilayer mirrors, creating the effect of a longer cavity.

Fig. 6b displays calculated values of the mode wavelength for cavity spacings from 0.5 to 3 μm. Although the cavity parameters used in the calculation yield slightly different absolute wavelength values, the same trends observed in Fig. 6a are apparent. Thus, the changes of the experimental mode wavelengths with increasing cavity spacing are understood.

4.3.3 Tuning the cavity spacing and modes with intracavity fluids

By translating the cavity, it is possible to tune the cavity spacing and consequently the emission wavelength. With fluid in the cavity, the emission intensity and linewidth can then be studied as a function of wavelength. This was done for both air (upper curve) and a laser dye (lower curve) in the cavity as displayed in Fig. 7. The solid points represent the measured emission intensity and the open points represent the measured linewidth.

The spectral intensity exhibits a peak near 850 nm and a dip near 840 nm. These correspond to well known emission and absorption features in AlGaAs/GaAs semiconductor materials. The maximum intensity in the dye-filled cavity is about 30 % higher than the corresponding maximum in the air cavity. Again, this is a manifestation of the higher index of the liquid. Effectively, the

liquid lowers the mirror reflectivities and allows more light out of the cavity.

Also shown in the figure are mode linewidths that decrease from 5 or 6 nm to 3 nm over the measured spectral range. The linewidth of the liquid-filled cavity appears to change increase more abruptly. This effect may be due to higher absorption caused by the dye. The details of these spectra are under further investigation.

5. CONCLUSIONS

In this paper we have presented some preliminary studies of fluids and their effects in semiconductor microcavities. The use of surface tension to transport fluid into a microcavity is simple, fast, and can be used with optical quality surfaces that have been prepared by separate epitaxial or deposition processes. Fluid volumes as small as 100 picoliters can be reproducible dispensed into the microcavity. Cavity filling times are the order of one second, and the fluid can be purged from the microcavity by gas pressure on the same time scale. The cavity can be used repetitively and can be easily opened, cleaned, and reassembled. The dynamics of fluid wetting can be monitored by observing cavity modes in the spontaneous emission spectrum excited by a pump laser. Details of mode wavelength dependence on cavity spacing and tuning effects were presented.

6. ACKNOWLEDGEMENTS

The authors gratefully acknowledge technical assistance and comments from T. French, A. E. Bieber, T. M. Michalske, N. A. Bixler, J. E. Bellum, A. J. Ricco, T. M. Brennan and B. E. Hammons. Work supported under DOE contract DE-AC04-94AL85000.

7. REFERENCES

1. See, for example, *Nanofabrication and Biosystems: Frontiers and Challenges*, Conference Program, Keauhou-Kona, Hawaii, May 8-12, 1994, Engineering Foundation Conferences, New York, 1994.
2. D. J. Harrison, K. Fluri, K. Seiler, Z. Fan, C. S. Effenhauser, and A. Manz, *Science* **261**, 895 (1993).
3. J. M. Ramsey, S. C. Jacobson, and M. R. Knapp, "Microfabricated Chemical Measurement Systems," *Nature Medicine* **1** 1093 (1995).
4. R. C. Anderson, G. J. Bogdan, R. J. Lipshutz. "Miniaturized genetic-analysis system," Solid-State Sensor and Actuator Workshop. Hilton Head, South Carolina, pp258-261, June 1996.
5. Microfabrication Technology for Biomedical Applications, October 24-25, 1996, San Jose, CA, Conference Notes, Cambridge Healthtech Institute, Upper Newton Falls, MA.
6. P. L. Gourley, *Nature*, October 13, 1994. P. L. Gourley, K. L. Lear, and R. P. Schneider, *IEEE Spectrum*, p 31-37, August, 1994.
7. *Selected Papers on Photodynamic Therapy*, David Kessel, Editor, Society of Photo-Optical Instrumentation Engineers, (Bellingham, WA, 1993), ISBN 0-8194-1268-2.
8. J. G. Fujimoto et al. Optical Biopsy an Imaging Using Optical Coherence Tomography, *Nature Medicine*, vol. 1, 970-972 (1995).
9. S. M. Block, in *Noninvasive Techniques in Cell Biology*, Chap. 15, Wiley-Liss (New York, 1990).
10. A. Ashkin and J. M. Dziedzic, *Science* **235**, 1517-20 (1987).
11. R. Wiegand-Steubing, S. Cheng, W. H. Wright, Y. Numajiri, and M. W. Berns, *Cytometry* **12**, 505-512 (1991).
12. H. M. Shapiro, in *Practical Flow Cytometry*, 2nd Ed., Alan R. Liss, Inc. New York, 1988.
13. P. L. Gourley, *Nature Medicine*, **2** 942 (1996).
14. P. L. Gourley et al., A Radically New Approach to Cell Structure Analysis, *Biophotonics International*, vol. 2, 48-56 (1995).
15. P. L. Gourley et al., Surface-emitting Semiconductor Laser Spectroscopy for Characterizing Normal and Sickled Red Blood Cells, *Advances in Laser and Light Spectroscopy to Diagnose Cancer and Other Diseases II: Optical Biopsy*, Proc. Biomedical Optics Society, SPIE vol. 2387, 148-161 (1995).
16. P. L. Gourley et al., Vertical Cavity Surface-emitting Laser Scanning Cytometer for High Speed Analysis of Cells, *Advances in Laser and Light Spectroscopy to Diagnose Cancer and Other Diseases III: Optical Biopsy*, Proc. Biomedical Optics Society, SPIE vol. 2679, 132-141 (1996).
17. R. Barer, *J. Opt. Soc. Am.* **47**, 545-52 (1957).
18. M. Andersen and S. Nir, *Polymer* **18**, 867-890 (1977).
19. R. P. Haugland, in *Handbook of Fluorescent Probes*, 5th edition, Molecular Probes, Inc. Eugene, OR (1992).

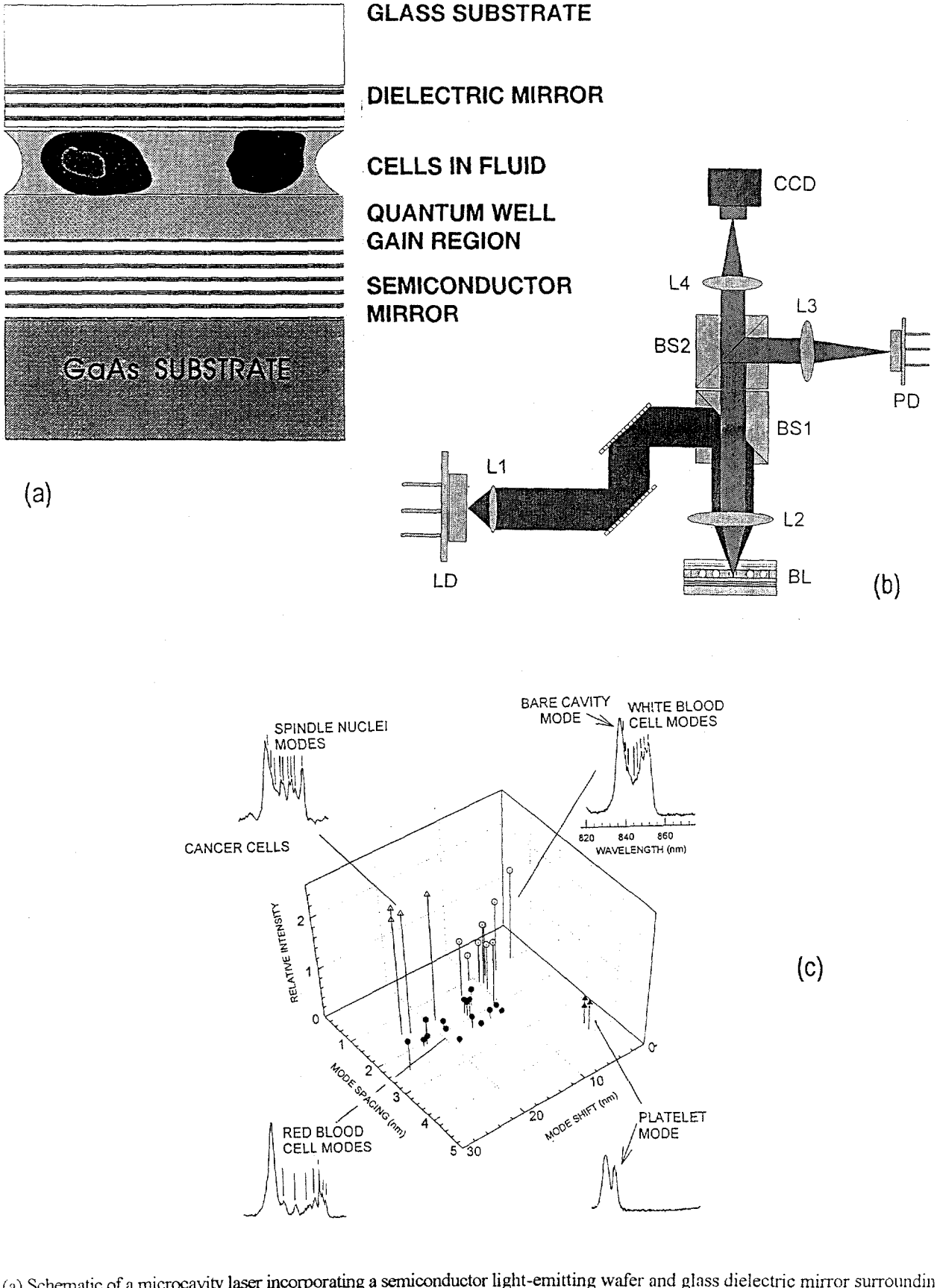

Fig. 1. (a) Schematic of a microcavity laser incorporating a semiconductor light-emitting wafer and glass dielectric mirror surrounding a biological fluid. (b) laser scanning method for reading information from the microcavity. (c) representative spectra for 4 different cell types and cluster plot for identifying cell types.

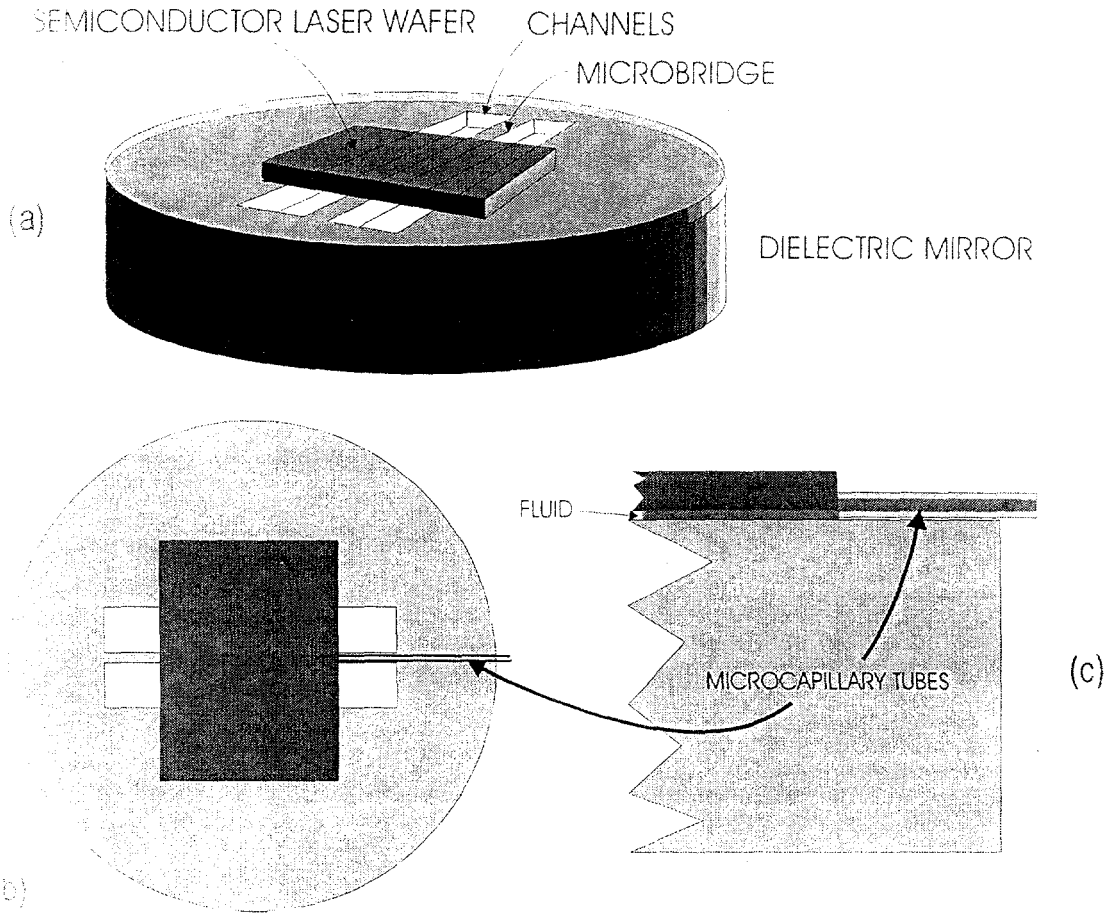

Fig. 2 Schematic of a microbridge fabricated inside the cavity to wick fluids from a microcapillary abutting the semiconductor wafer (a) perspective view, (b) top view and (c) side view.

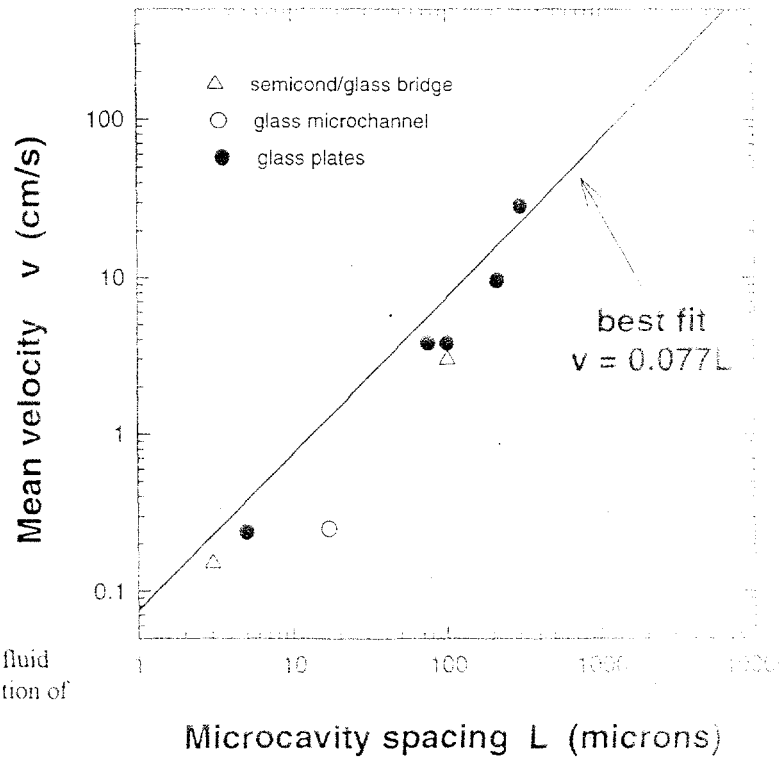

Fig. 3 Measured average velocity of intracavity fluid in three different microcavities as a function of cavity spacing.

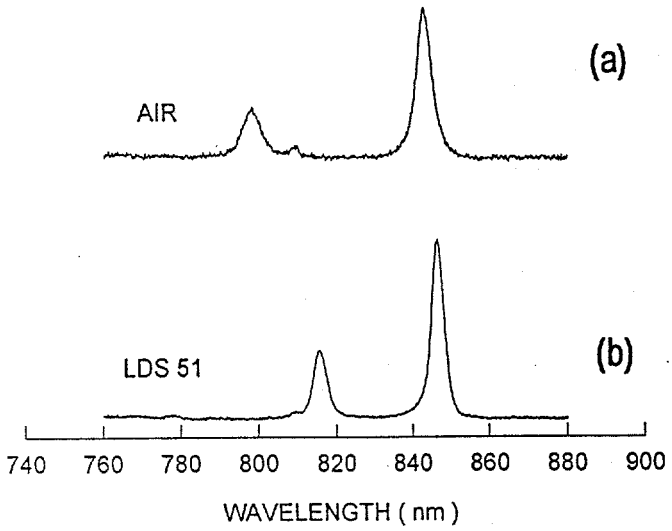

Fig. 4. Typical emission spectra from the semiconductor/ glass microcavity filled with (a) air, and (b) laser dye LDS751 in ethylene glycol.

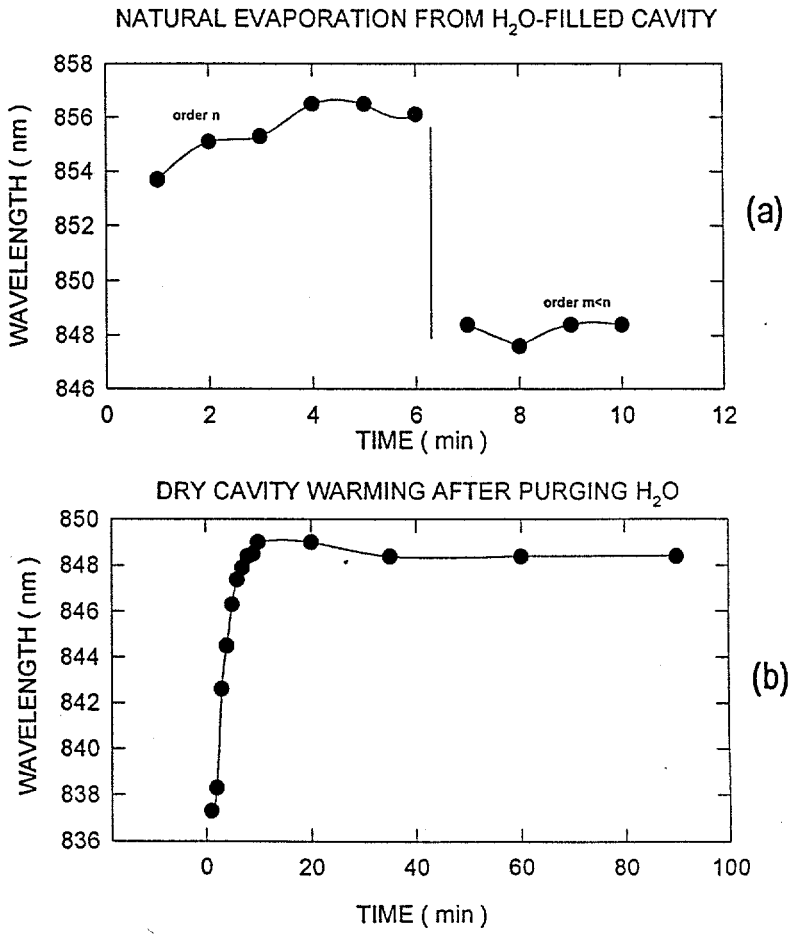

Fig. 5. Dynamics of cavity modes showing the time changes of a longitudinal mode during (a) natural evaporation of water, and (b) warming after a pressurized gas purge.

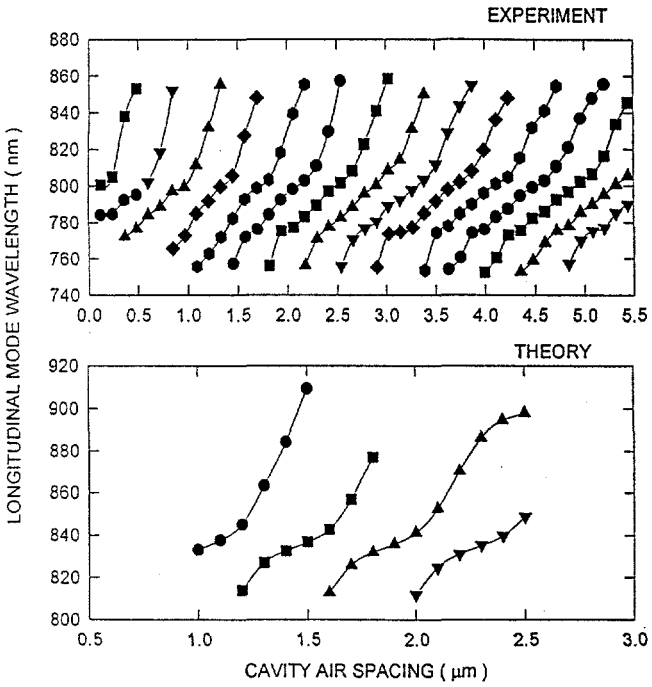

Fig. 6. (a) Experimentally determined mode wavelengths as a function of cavity spacing and (b) theoretical mode wavelengths as a function of intracavity air spacing.

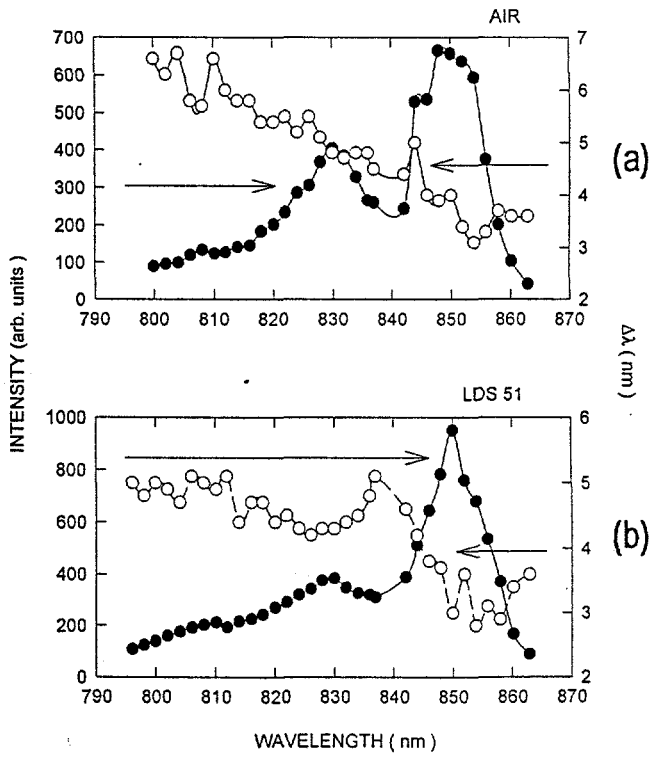

Fig. 7. (a) Spectral tuning curves for air and (b) laser dye LDS751. The cavity emission intensity (solid points) and linewidth (open points) are displayed.